#### Research Article

Meiyi Gao, Haitao Zhang\*, Yongcai Gu\*, Song Zhao, Zhichao Guo, and Yuchen Li

## Effects of freeze-thaw cycles on micro and mesostructural characteristics and mechanical properties of porous asphalt mixtures

https://doi.org/10.1515/rams-2023-0116 received January 16, 2023; accepted August 28, 2023

Abstract: Porous asphalt concrete (PAC) have a typical big void-skeleton structure, and porous asphalt mixtures with large voids are more prone to freeze-thaw damage. As a result, research on the influence of freeze-thaw cycles on the micro-structure and mechanical characteristics of porous asphalt mixes offers a theoretical framework for overcoming water stability concerns in porous asphalt mixtures in practice, as well as for further popularization and application. In this study, styrene-butadiene-styrene (SBS)modified asphalt and high viscosity modified asphalt were constructed on the basis of the original asphalt, and the mix proportions of asphalt mixes PAC-13, AC-13, and SMA-13 were designed. To begin, molecular dynamics simulations were used to look into the effects of freeze-thaw cycles on asphalt-aggregate interface adhesion and mixture micromechanical properties. Second, the effects of freeze-thaw cycles on the void characteristics of porous asphalt mixtures were explored utilizing digital image processing technologies. Finally, the freeze-thaw split test was utilized to evaluate the macroscopic mechanical properties of a porous asphalt mixture after freezing and thawing cycles. According to the study findings, high viscosity modified asphalt made with 4% SBS/8% TPS has the greatest performance. The application of SBS/TPS-modified asphalt can considerably improve the damage resistance of porous asphalt mixes. The microstructure and mechanical qualities of porous asphalt mixtures are damaged by freeze-thaw cycles, and the damage gets worse as the number of cycles rises. The study's conclusions provide a theoretical justification for the application of porous asphalt pavement.

**Keywords:** porous asphalt mixture, freeze, thaw cycle, molecular simulation, micro and meso-structure, mechanical properties

#### Nomenclature

PAC	porous asphalt concrete
AC	asphalt concrete
SBS	styrene–butadiene–styrene
SMA	stone mastic asphalt
TPS	tafpack super
SBS/TPS-modified	SBS and TPS two modifiers composite
asphalt	modified asphalt
orginal asphalt	unmodified asphalt
OGFC	open-grade friction courses
PA	porous asphalt
RAP	reclaimed asphalt pavement
CR	crumb rubber
Penetration	indicators of the relative viscosity of
	asphalt
Softening point	the temperature at which asphalt
	begins to soften and lose its solid
	properties during the heating process
Ductility	ductility of asphalt

e-mail: zht6781@163.com

**Meiyi Gao, Song Zhao, Zhichao Guo:** College of Civil Engineering, Northeast Forestry University, Harbin, 150040, China

Yuchen Li: Campus Construction Division, Northeast Forestry University, Harbin, 150040, China

#### 1 Introduction

Dynamic viscosity

Because of its superior smoothness, driving comfort, and ease of construction and maintenance, asphalt pavement has become the most popular form of pavement on today's metropolitan roads and highways. Traditional asphalt pavement material selection and structural design is

reflective asphalt

indicators of heat resistance of

<sup>\*</sup> Corresponding author: Haitao Zhang, College of Civil Engineering, Northeast Forestry University, Harbin, 150040, China,

<sup>\*</sup> Corresponding author: Yongcai Gu, College of Civil Engineering, Northeast Forestry University, Harbin, 150040, China, e-mail: Guyongcai2005@sohu.com

<sup>👸</sup> Open Access. © 2023 the author(s), published by De Gruyter. 😥 💌 This work is licensed under the Creative Commons Attribution 4.0 International License.

Porous asphalt pavement is composed of an opengraded asphalt mixture with significant voids, ranging from 18 to 22% void ratio. Varied countries place different emphasis on the functional aspects of porous asphalt pavement. As a result, nations are labeled based on their structural kinds, functional attributes, and uses. It is known as porous asphalt concrete (PAC) in Europe, open-graded friction course (OGFC) in the United States, porous asphalt (PA) in Japan, and so on [6]. Because of its functional features, porous asphalt pavement has been popular and widely used in many nations and areas. Foreign professionals have now conducted extensive study on porous asphalt mixtures, yielding particular research outcomes. Meiarashi et al. [7] investigated the noise reduction properties of porous asphalt pavement. The results reveal that, when different types of vehicles pass by, the porous asphalt pavement has a greater noise reduction impact than the typical densely dispersed asphalt pavement, and the noise reduction effect is optimum when the pavement porosity is around 20%. Water permeability of porous asphalt pavement was examined by Dreelin and colleagues [8]. The findings suggest that porous asphalt pavement has major technical importance for managing road surface water and surface runoff concerns. Goh and You [9] looked into the mechanical properties of regenerated porous asphalt pavement. Two additives, reclaimed asphalt pavement (RAP) and warm mix asphalt (WMA), were used to regenerate the asphalt pavement, and a range of mechanical indexes of the regenerated asphalt mixture were studied in laboratory

testing. The asphalt mixture regenerated with 15% RAP and 0.25% WMA has the best mechanical qualities, according to the data. Shirini and Imaninasab [10] compared the mechanical and functional qualities of PA mixes with varying rubber powder concentrations.

The results suggest that rubber powder and styrenebutadiene-styrene (SBS) may considerably improve the mechanical and anti-skid qualities of PA asphalt mixtures, but too much rubber powder has a negative impact, and the addition of rubber particles is not beneficial to PA mixtures. Drainage properties: Chen et al. [11] investigated the engineering parameters of PAC asphalt mixes in the laboratory and in the field. The permeability, rutting resistance, disintegration resistance, and other engineering qualities of PAC were investigated in laboratory testing, and a test road was established to monitor performance based on the assessment results. The results demonstrate that the modified asphalt mixture has better mechanical qualities and drainage characteristics than conventional asphalt. Islam et al. [12] investigated the performance of two graded asphalt mixes, asphalt concrete (AC) and OGFC, at low temperatures. By measuring indirect tensile strength, thermal shrinkage coefficient, and dynamic modulus, the low temperature transverse cracking potential of AC and OGFC was determined. The results reveal that OGFC has more ductility and creep flexibility than AC [13], demonstrating that OGFC is one of the best materials for preventing lateral cracking of pavement in low temperature regions. PAC-16 asphalt mixture with limestone aggregate was produced by Xu et al. [13], who also looked at its mechanical and drainage properties. The results demonstrate that the limestone PAC-16's indoor and outdoor performance is consistent with the requirements, supporting the use of limestone aggregate in the lower layer of a double-layer porous asphalt pavement. Yang et al. [14] produced SBS/tafpack super (TPS)-modified asphalt with SBS and crumb rubber modifiers and investigated the high-temperature, fatigue, and low-temperature characteristics of PAC asphalt mixture. The results show that the high viscosity modified asphalt significantly improves the mechanical properties of the asphalt mixture. Aliha et al. also showed that the addition of modifiers to asphalt mixes can effectively improve the fracture toughness of asphalt mixes [15].

However, there are certain inconsistencies between the mechanical and functional qualities of porous asphalt mixes. Since the functional features of porous asphalt mixes are based on the existence of more pores than strictly graded asphalt mixtures, they have lower structural strength. Mansour and Putman discovered that the indirect tensile strength and durability of porous asphalt mixes decreased with increasing porosity [16]. Slebi-Acevedo *et al.*  tested fracture energy and toughness variations by adding synthetic fibers to porous asphalt mixes. Test results showed that the incorporation of synthetic fibers could improve the toughness and ductility of porous asphalt mixtures [17]. Lebens and Troyer have shown that porous asphalt mixes are weaker and more vulnerable to environmental influences (e.g., freeze-thaw cycle effects) than densely formed asphalt mixtures, such as densely formulated hot-mix asphalt mixtures [18]. Relevant research has also revealed that environmental factors influence the performance of materials in use. Ghoreishian Amiri et al., for example, developed an elasto-plastic intrinsic model to study the fluctuation of basic permafrost features [19].

In summary, this study selected to create porous asphalt mixes with high viscosity modified asphalt to increase their low temperature cracking resistance. Molecular dynamics modeling was used to evaluate and analyze the study's findings. Molecular dynamics simulation technology is used to mimic the adhesion of the asphalt-aggregate interface during freeze-thaw cycles as well as the mechanical properties of the mixed specimens after freeze-thaw cycles. The PAC-13, SMA-13, and AC-13 asphalt mixture specimens were made using the original asphalt, SBS-modified asphalt, and high viscosity modified asphalt, respectively. The effect of freeze-thaw cycles on the pore characteristics of porous asphalt mixtures was examined at the mesoscopic level using digital image processing technology. Finally, a freezethaw splitting test was used to look at the macroscopic mechanical properties of a porous asphalt mixture after freeze-thaw cycles. It could be useful for protecting porous asphalt mixes from water damage.

At the same time, the majority of current research on the impacts of freeze-thaw cycling on asphalt mixes has concentrated on the macroscopic changes in characteristics rather than the microscopic elements of interior damage. There has been no investigation into damage processes at the molecular level. There has also been no study on molecular modeling to develop a structural model of water molecules encapsulating asphalt mixes, which cannot be realistically constructed in freeze-thaw cycle conditions. As a result, the study presented in this work establishes a research

foundation for the damage process of asphalt mixes (particularly porous asphalt mixtures) in freeze-thaw cycle settings at the microscopic scale.

#### 2 Materials and methodology

#### 2.1 Test material and mixture proportion design

#### 2.1.1 Asphalt

First, raw asphalt was utilized, and SBS modifier was used to create 4% SBS-modified asphalt. On this premise, an 8% TPS modifier was added to the asphalt to increase its viscosity, resulting in a high viscosity composite modified asphalt. Table 1 displays the asphalt indications.

#### 2.1.2 Aggregate

This study compares PAC-13 and AC-13 with SMA-13 as the research object. The gradation curves of PAC-13, AC-13, and SMA-13 are depicted in Figure 1.

#### 2.1.3 Mixture proportion design

The change law of mechanical characteristics under freezethaw cycles was investigated using experimental analysis for the PAC-13, AC-13, and SMA-13. To manufacture molded asphalt mixes in this investigation, 4% SBS-modified asphalt and 4% SBS/8% TPS composite SBS/TPS-modified asphalt were employed. The ideal asphalt dosages of PAC-13, AC-13, and SMA-13 for 4% SBS-modified asphalt are 4.3, 4.9, and 5.8%, respectively; for high viscosity modified asphalt, the optimum asphalt dosages of PAC-13, AC-13, and SMA-13 are 4.6, 5.2, and 6.4%, respectively. SMA-13 and PAC-13 received 0.3% lignin fibers and 0.4% basalt lithofibers, respectively, based on gradation properties.

Table 1: Asphalt technical indicators

Asphalt	Penetration/25°C (0.1 mm)	Softening point/°C	Ductility/5°C (mm)	Dynamic viscosity/60°C (Pa·s)
Original asphalt	84.3	44.8	120	197
4% SBS-modified asphalt	58.7	78.5	233	24,540
4% SBS/8% TPS-modified asphalt	45.6	91.4	356	34,253

4 — Meiyi Gao et al. DE GRUYTER

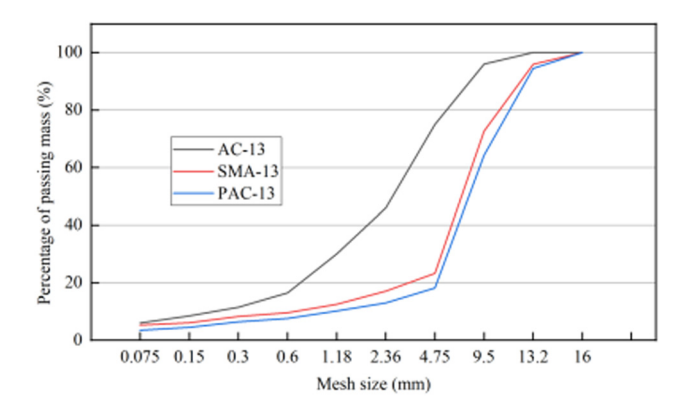


Figure 1: Gradation curve of asphalt mixture.

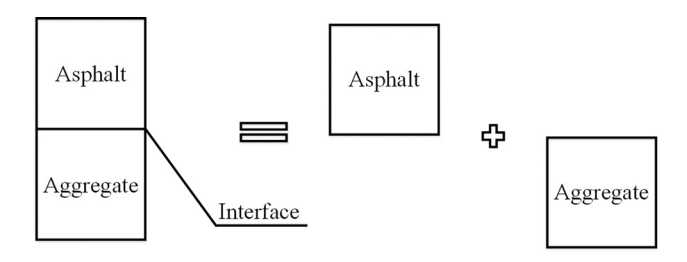


Figure 2: Schematic diagram of interface energy.

#### 2.2 Test methodology

#### 2.2.1 Molecular dynamics simulation

Interface energy is calculated in the same way as surface energy [20], but it varies from surface energy in that it indicates the strength of the interface contact between two distinct materials. Figure 2 depicts the calculation diagram.

When an interlayer structure is separated into upper and lower sections, the intermediate interface forms two surfaces, causing energy shifts that might indicate the strength of the interface contact. The following formula (1) was used to calculate the interface energy between asphalt and aggregate:

$$E_{\text{Inter}} = (E_{\text{Asphalt}} + E_{\text{Aggregate}}) - E_{\text{Total}},$$
 (1)

where  $E_{\rm Inter}$  is the interface energy between the two-layer systems,  $E_{\rm Total}$  is the total energy of the two-layer system (including asphalt system and aggregate system),  $E_{\rm Asphalt}$  is the energy of the asphalt system, and  $E_{\rm Aggregate}$  is the energy of the aggregate system.

That is, the energy of the interface between the two phases is equal to the sum of the energies of the two phases subtracted from the energies of the two phases as a whole. Furthermore, every system is stressed in molecular dynamics calculations due to the impact of an external force, causing the relative locations of particles in the system to change [21]. The stress—strain behavior of the complete asphalt mixing system may be fully characterized using only two independent coefficients. The system's Poisson's ratio  $\nu$ , Young's modulus E, bulk modulus E, and shear modulus E are stated as follows:

$$v = \frac{\lambda}{2(\lambda + \mu)} \quad E = \frac{\mu(3\lambda + 2\mu)}{\lambda + \mu} \quad K = \lambda + \frac{2}{3}\mu \quad G = \mu. \quad (2)$$

#### 2.2.2 Digital image processing

Digital image processing refers to the methods and technologies used to convert images into digital signals and improve processing. Image enhancement, suppression, and geometric alteration are all examples of digital image processing that can improve image visual quality [22]. On this basis, numerous picture characteristics and specific information, and the relevant performance in the test are eventually assessed using the image information. SBS/TPS-modified asphalt is used in this work to create PAC-13 asphalt mixture specimens, which are then freeze—thaw cycle maintained. Using a high-precision scanner, a cross-sectional image of the material is created, which is then digitally processed and evaluated for void characteristics. The specific approach is depicted in Figure 3.

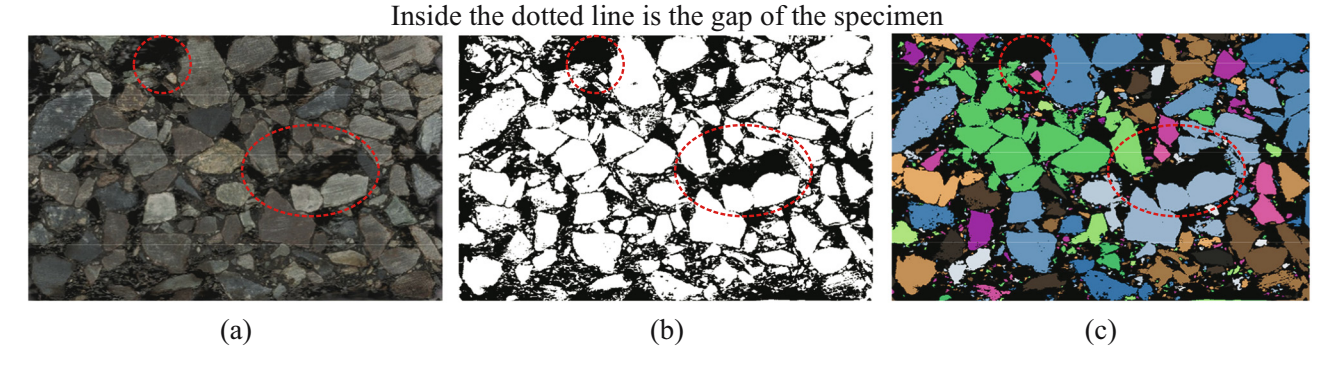


Figure 3: Process of digital image processing: (a) specimen section, (b) digital processing, and (c) parameter analysis.

#### 2.2.3 Freeze-thaw split tests

Examples of freeze-thaw cycles include vacuum saturated water, freeze-swell, and high-temperature water bath operations. Several freeze-thaw cycles may be used to better assess the durability of asphalt mixtures during long-term freeze-thaw cycles. Freeze-thaw cycles can cause interior structural damage in asphalt mixes. This is reflected in increased porosity and decreased mechanical characteristics. As a consequence, PAC-13, AC-13, and SMA-13 were used to perform freeze-thaw split experiments in this work, and the mechanical properties of the material were studied during the freeze-thaw cycles. Three specimens were prepared for each asphalt mixture during the freeze-thaw cycle, and the test results were averaged to eliminate the effect of errors. The number of freeze-thaw cycles in this article was set to 0, 1, 3, 6, 9, 12, and 15. This article referred to the experimental method in China's "Test Procedure for Asphalt and Asphalt Mixture in Highway Engineering" (JTGE20-2011). That is, it was frozen at -18°C for 16 h, then thawed at 60°C for 8 h, and finally stood at room temperature for 2 h as part of a freeze-thaw cycle.

# 3 Effects of freeze-thaw cycles on the micro-structures of porous asphalt mixes

#### 3.1 Establishment of model

#### 3.1.1 Molecular model of asphalt

Li and Greenfield [23] suggested AAA-1 asphalt. SBS modifier is a two-phase separation SBS triblock copolymer that

can increase the temperature sensitivity and viscosity of asphalt. TPS modifiers, on the other hand, have a complicated composition that includes a range of polymers, and there is no unique molecular structure model. As a result, a molecular model of SBS/TPS-modified asphalt was built with double the amount of SBS modifier, and simulation study was conducted. Figure 4 depicts the molecular composition. Table 2 shows the exact molecular makeup.

#### 3.1.2 Molecular model of aggregate

The acid aggregate has a  $SiO_2$  content of more than 65%, whereas the alkaline aggregate has a  $SiO_2$  content of less than 52% [23]. The material used in this experiment is acid granite aggregate. The particular component composition is shown in Table 3. In this paper, silicon dioxide crystal units were subjected to cell expansion to construct silicon

Table 2: Molecular composition of modified asphalt

Molecular structure	Chemical formula	Number	Molar mass (g∙mol <sup>−1</sup> )
Asphaltene-pyrrole	C <sub>66</sub> H <sub>81</sub> N	888	2
Asphaltene-phenol	$C_{42}H_{54}O$	575	3
Asphaltene-thiophene	$C_{51}H_{62}S$	707	4
Pvridinohopane	$C_{36}H_{57}N$	503	2
Quinolinohopane	$C_{40}H_{59}N$	554	2
Thioisorenieratane	$C_{40}H_{60}S$	573	2
Benzobisbenzothiophene	$C_{18}H_{10}S_2$	290	3
Trimethylbenzeneoxane	$C_{29}H_{50}O$	414	15
DOCHN	$C_{30}H_{46}$	406	21
PHPN	C <sub>35</sub> H <sub>44</sub>	464	18
Squalane	$C_{30}H_{62}$	422	7
Hopane	$C_{35}H_{62}$	483	7
SBS	$C_{29}H_{40}$	388	4
TPS	$C_{29}H_{40}$	388	12

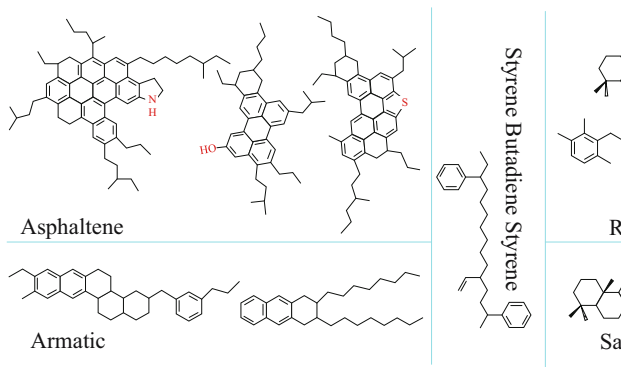


Figure 4: Molecular formulas of asphalt components and modifiers.

Table 3: Chemical composition of aggregate

Aggregate		Main oxide content (%)							
	SiO <sub>2</sub> CaO Al <sub>2</sub> O <sub>3</sub> Fe <sub>2</sub> O <sub>3</sub> MgO Others								
Granite	76.56	0.85	10.52	0.61	0.09	11.37			

dioxide structure models. The aggregate model is depicted in Figure 5.

### 3.1.3 Establishment of model based on freeze-thaw cycle system

Start by using the Geometric Optimization function in the Forcite section, selecting the COMPASS force field, and setting the maximum number of iterations to 100,000 to guarantee that the model converges and the energy is decreased. The annealing process is then carried out on the Forcite plate by selecting the COMPASS force field, the NVT ensemble, 300–1,500 K, and 15 cycles. For additional investigation and analysis, kinetic simulations of the annealed interface model were performed. The model was run at 298 K for 200 ps on the Forcite plate, and the model's trajectory information was generated every 5,000 steps. At this point, the asphalt–aggregate contact becomes stable. Build an equal area surrounding the asphalt–aggregate

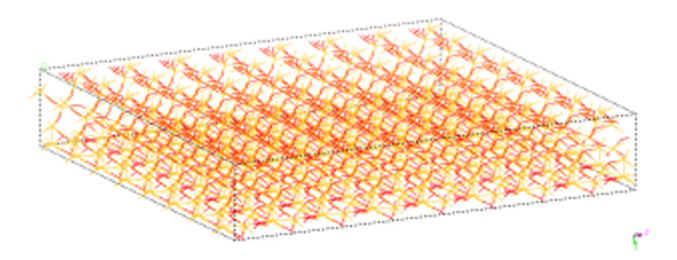


Figure 5: Aggregate molecular model.

model and fill the vacuum layer with water molecules to create a freeze-thaw cycle system model. Figure 6 shows the construction process using SBS-treated asphalt as an example.

#### 3.2 Simulation results

#### 3.2.1 Interface energy

The influence of freeze-thaw cycles will result in some asphalt mixture deterioration. This is because, as water enters the voids of the asphalt mixture, a certain water pressure is generated under the action of temperature and load, and it will invade the interface between asphalt and aggregate, causing asphalt emulsification, the viscosity of asphalt decreases, the interface adhesion decreases, and eventually it gradually develops into a serious pavement disease, kinetic calculations for three different asphalt-aggregate systems under frost conditions [24]. Under the constantpressure, constant-temperature ensemble, the pressure is standard air pressure (0.0001 GPa), the temperature is 255 K (-18°C), the low temperature operation is done for 160 ps, and the high temperature operation is performed at 333 K (60°C) twice as one cycle. There are a total of five instances. According to the molecular simulation in this research, the interface energy value is negative, suggesting that there is adhesion between asphalt and aggregate. The greater the absolute value, the more strongly the surface asphalt adheres to the aggregate. Table 4 displays the interface energy created by freeze-thaw cycles between the three asphalts and aggregates.

Table 4 demonstrates how the absolute value of the interface energy between asphalt and aggregate decreases as the number of freeze—thaw cycles rises. Think about the energy transfer that occurs during freeze—thaw cycles at the interface between aggregate and SBS/TPS-modified asphalt. The interface energy between asphalt and

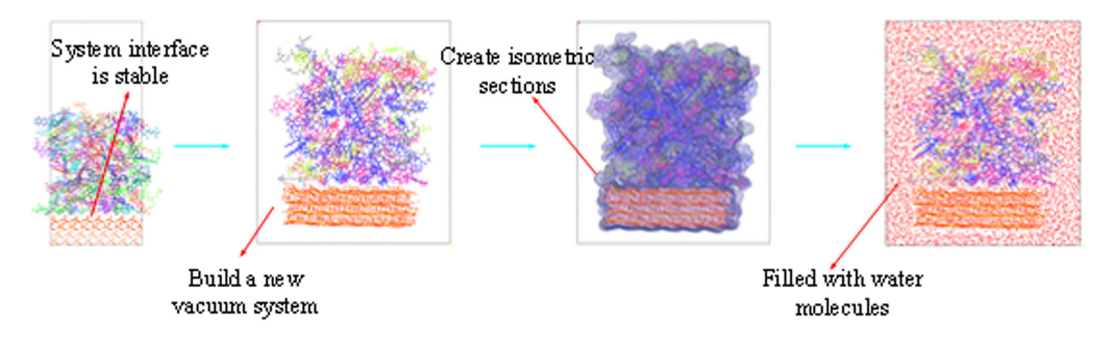


Figure 6: Molecular model of freeze-thaw cycles.

**Table 4:** Interface energy of asphalt–aggregate under freeze–thaw cycles (kJ·mol<sup>-1</sup>)

Number of	Asphalt–aggregate					
freeze-thaw cycles (times)	Original asphalt	SBS- modified asphalt	SBS/TPS- modified asphalt			
1	-2177.2	-3328.1	-3936.5			
2	-2052.3	-3056.5	-3817.6			
3	-1918.6	-2879.1	-3729.3			
4	-1853.4	-2614.2	-3614.1			
5	-1632.1	-2314.5	-3534.7			

aggregate is 3936.5 kJ·mol<sup>-1</sup> in absolute terms after one freeze–thaw cycle, and it decreases by 5.3 and 10.2% after three and five freeze–thaw cycles, respectively, to 3729.3 and 3534.7 kJ·mol<sup>-1</sup>. This shows that freeze–thaw cycles reduce asphalt–aggregate adhesion, and that the attenuation rises with an increase in the frequency of freeze–thaw cycles.

The energy of the asphalt–aggregate contact through numerous freeze–thaw cycles is shown in Figure 7. The absolute value of the interface energy between high viscosity modified asphalt and aggregates in the same environment and for the same aggregate is found to be significantly higher than that of SBS-modified asphalt and aggregates and original bitumen and aggregate when the interface energies of various asphalts and aggregates are compared. The absolute values of the interface energy between the original asphalt and the SBS-modified asphalt are 1632.1 and 2314.5 kJ·mol<sup>-1</sup>, respectively, in the freeze–thaw cycle

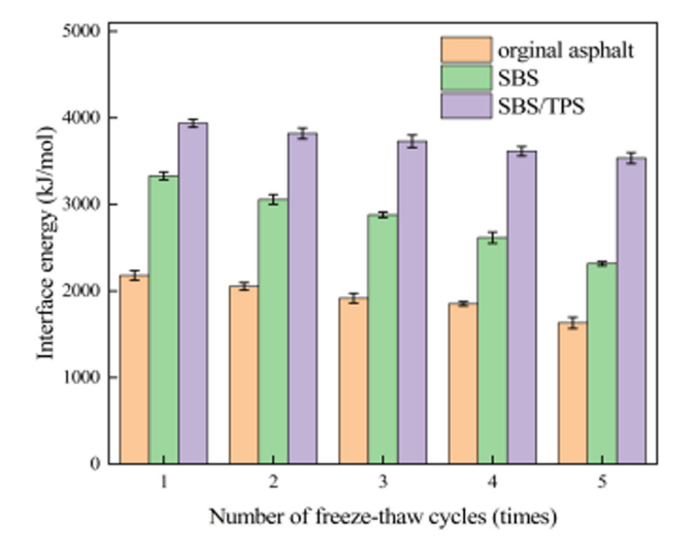


**Figure 7:** Interface energy between different asphalt–aggregate under freeze–thaw cycles.

results. Under the same conditions, the high viscosity changed asphalt's interface energy and the aggregate is 3534.7 kJ·mol<sup>-1</sup>, which is 2.2 times as large as the original asphalt and 1.5 times as large as the SBS-modified asphalt. This reveals that when subjected to freeze—thaw cycles, the SBS/TPS-modified asphalt adhered to aggregates more effectively than both the original asphalt and the SBS-modified asphalt.

According to earlier research, the number of freezethaw cycles affects the interface energy (also known as adhesion) between asphalt and aggregate in the molecular dynamics simulation. When there is no adhesion at the asphalt-aggregate interface, moisture deterioration of the interface occurs, ultimately causing the separation of the molecules of asphalt and aggregate. Figure 8 illustrates, using the initial asphalt-aggregate interface gap as an example, how more water molecules enter the asphaltaggregate interface when the frequency of freeze-thaw cycles rises, leading to asphalt failure. Meanwhile, the study's research team discovered that water molecules can fight for electrons surrounding the aggregates. This permits water molecules to build new chemical connections with the aggregate by breaking the chemical bonds made between the asphalt components and the aggregate. This causes moisture to infiltrate the asphalt-aggregate contact [25]. The interfacial energy between asphalt and aggregate is eventually lowered. Furthermore, water penetrating the asphalt-aggregate contact steadily rises in volume as it freezes, resulting in frost heave. This exacerbates the damage to the asphalt-aggregate contact and weakens the interfacial energy once again.

The macroscopic properties of the asphalt mixture eventually deteriorate as the distance between asphalt molecules and aggregate molecules grows and the strength of bonding declines.

#### 3.2.2 Analysis of mechanical properties

The modulus was developed by allowing the atoms in the molecular model to move freely. Second, the molecular model of the mixture was extended in all directions during the computation of mechanical properties [26]. At this point, the relative placement of the particles in the system changes, as does the modulus. This simulation is based on the findings of Lamé's constant, taking into consideration all the aforementioned variables and the diversity of simulated outcomes (assuming that the material is isotropic). When the mechanical characteristics of the asphalt mixture system were simulated after five freeze—thaw cycles, each system (Table 5 and Figure 9) shows Poisson's ratio ( $\nu$ ), Young's modulus (E), bulk modulus (E), and shear modulus (E).

8 — Meiyi Gao *et al.* DE GRUYTER

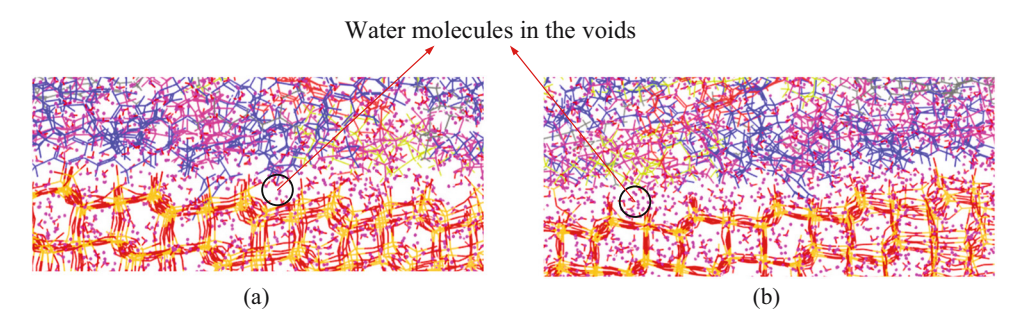


**Figure 8:** Degree of binding between asphalt and aggregate under different freeze–thaw cycles: (a) one time of freeze–thaw cycle and (b) five times of freeze–thaw cycles.

**Table 5:** Results of mechanical properties of asphalt mixture system after five times of freeze-thaw cycle

Asphalt mixture system	λ	μ	ν	<i>E</i> (GPa)	<i>K</i> (GPa)	<i>G</i> (GPa)
Original asphalt SBS-modified	1.33 1.54		0.25 0.24	3.39 4.07	2.24 2.63	1.36 1.64
asphalt SBS/TPS-modified asphalt	1.70	1.74	0.25	4.34	2.86	1.74

Table 5 and Figure 9 demonstrate that although the Young's modulus, bulk modulus, and shear modulus of the SBS/TPS-modified asphalt mixture change significantly

after five freeze—thaw cycles, the Poisson's ratio of the three sets of the systems does not. The SBS-modified asphalt mixture has a higher shear modulus than the original asphalt mixture system. It illustrates that when subjected to freeze—thaw cycles, the SBS/TPS-modified asphalt combination possesses the necessary mechanical properties. This is because the combination of SBS modifier and TPS modifier increases the modulus of the modified asphalt even further.

Meanwhile, when the modulus of asphalt was compared after different numbers of freeze—thaw cycles, it was discovered that the freeze—thaw cycles steadily increase the modulus of asphalt. As a result, the asphalt becomes harder and more brittle, making it unsuitable for usage in low-temperature conditions.

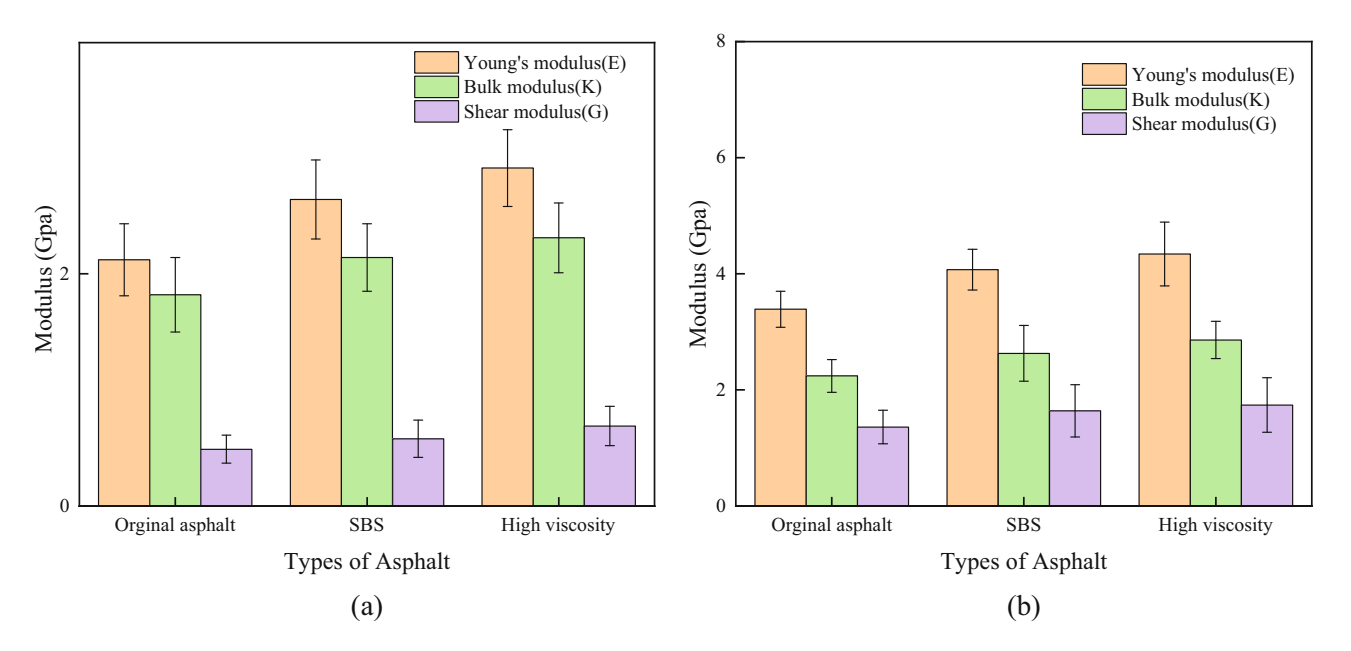


Figure 9: Modulus after different number of freeze-thaw cycles: (a) modulus without freeze-thaw cycles and (b) modulus after five freeze-thaw cycles.

# 4 Analysis of meso-structural properties

# 4.1 Section acquisition and digital image processing

The PAC-13 mixed specimens were created with SBS/TPS-modified asphalt, cut into semi-circular forms, and tested using freeze—thaw cycles. A high-precision scanner with a resolution of 1,200 dpi was used to scan the cured semi-circular specimen in cross-section. Figure 10 shows the digital image processing.

The scanned pictures must be further processed in order to help the PCAS software detect the voids in the mixture and acquire the required parameters of the void characteristics more precisely. The highest class variance value method is employed in Python's digital image processing technology to accomplish picture segmentation on the global threshold [27,28]. Formula (3) depicts the threshold segmentation principle:

$$F(x,y) = \begin{cases} 1, g(x,y) \ge T \\ 0, g(x,y) < T \end{cases} \quad X = \omega_1 x_1 + \omega_2 x_2. \tag{3}$$

In formula (3), F(x,y) is the image after segmentation, g (x,y) is the image before segmentation, T is the threshold, X is the total average gray level of the image,  $\omega_1$  and  $\omega_2$  are the proportion of effective points in the foreground pattern and the effective proportion of the background pattern, respectively, and  $x_1$  and  $x_2$  are the average gray levels of the foreground and background, respectively. When the inter-class variance value  $G = \omega_1(x - x_1)^2 + \omega_2(x - x_2)^2$ reaches the maximum, the difference between the foreground and the background is the largest, and the generated image has the best effect, which can more clearly reflect the mesoscopic view of the mixture. The thresholded images were imported into PCAS for void identification and related parameter analyses to obtain the characteristics of the changes in the internal pores of asphalt mixtures after different numbers of freeze-thaw cycles.

#### 4.2 Analysis of void size and quantity

The PAC-13 asphalt mixture picture was processed using Python threshold and void identification and statistical analysis was done using PCAS's void identification function. Figure 11 depicts digital pictures of PAC-13 asphalt

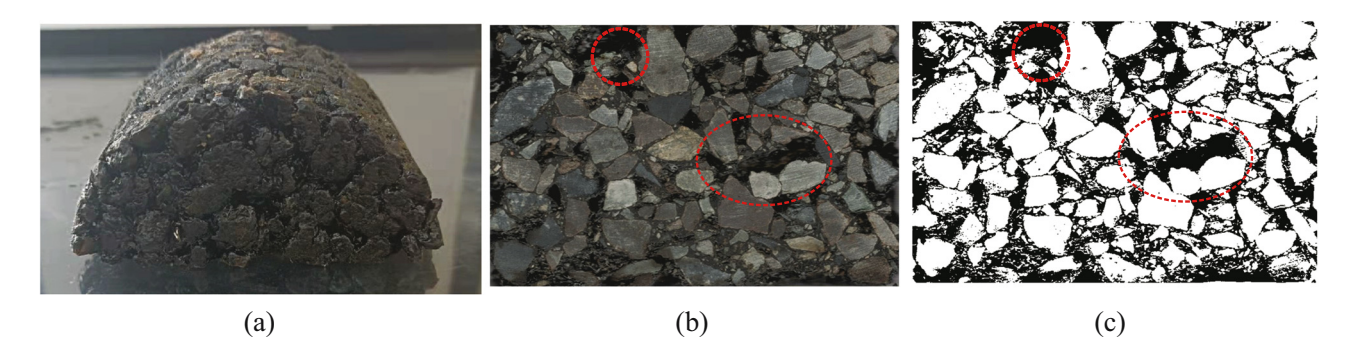


Figure 10: Digital image processing: (a) specimen scanning, (b) scanning image, and (c) image processing.

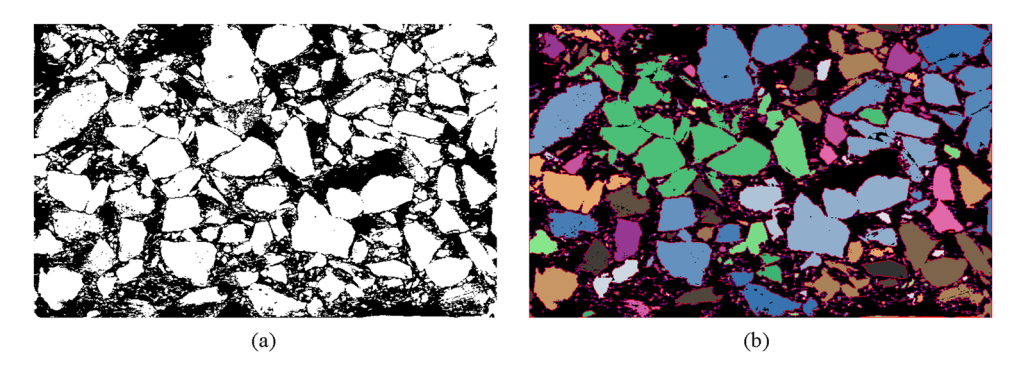


Figure 11: Digital images of PAC-13 under freeze-thaw cycles: (a) image after threshold segmentation and (b) PCAS image recognition.

Table 6: Void eigenvalues

Specimen handling	Void area (mm²)	Number of gaps	Void ratio (%)	Maximum length (mm)	Maximum width (mm)
Before freeze–thaw cycle	1,528	503	19.4	8.42	6.02
After freeze-thaw cycle	1,745	737	21.6	9.65	7.34

mixture under various water-temperature coupling settings, and Table 6 depicts significant characteristic data such as void area and perimeter.

Table 6 demonstrates that as compared to the specimens prior to freeze—thaw cycles, the void area of the samples rose by 14.2%, and the number of voids increased by 46.5%. Following the freeze—thaw cycle treatment, the maximum length and maximum breadth of the mixed specimens increased. During the freeze—thaw cycle, the specimen's internal structure is compromised, increasing the quantity of voids and the border's size. The asphalt mixture exhibits a porous medium structure [29] with closed

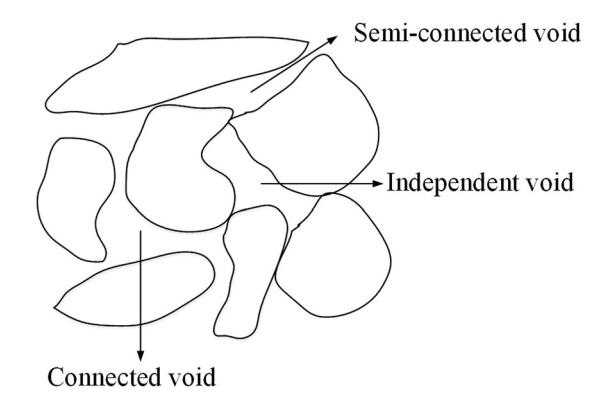


Figure 12: Types of voids in asphalt mixture.

gaps, semi-connected voids, and linked voids, as shown in Figure 12. The analysis of its void changes contributes to mesoscopic knowledge of how freeze—thaw cycles affect the performance of asphalt. As a consequence, the cross-section pores were eliminated and placed in the same layer at the same scale utilizing digital image technology. Figure 14 shows a part of the extraction results.

Figure 13 shows the PAC-13 asphalt mixed specimen after the freeze-thaw cycle, since the water freezes from the outside to the inside at low temperatures, the frozen water inside cannot break through the ice seal layer outside the exterior specimen, thus the water is frozen. The freeze-swell pressure works on the interior of the mixture, penetrating some voids' weak points. When the hot water bath melts, the water flow enters these weak places, speeding up the peeling of the asphalt off the aggregate and expanding the length and area of the pores. Figure 14 displays a scatter plot of the border characteristics of the PAC-13 asphalt mixture voids. The increase in voids in the PAC-13 asphalt mixture following the freeze-thaw cycle is seen in Figure 14. The process caused the voids in the PAC-13 asphalt mixture to grow in length and breadth. The figure shows that the number of voids that exceed the limit after the freeze-thaw cycle is mainly, using 2 mm × 2 mm as the void size limit. This indicates that the asphaltaggregate adhesion interface will be disrupted by the

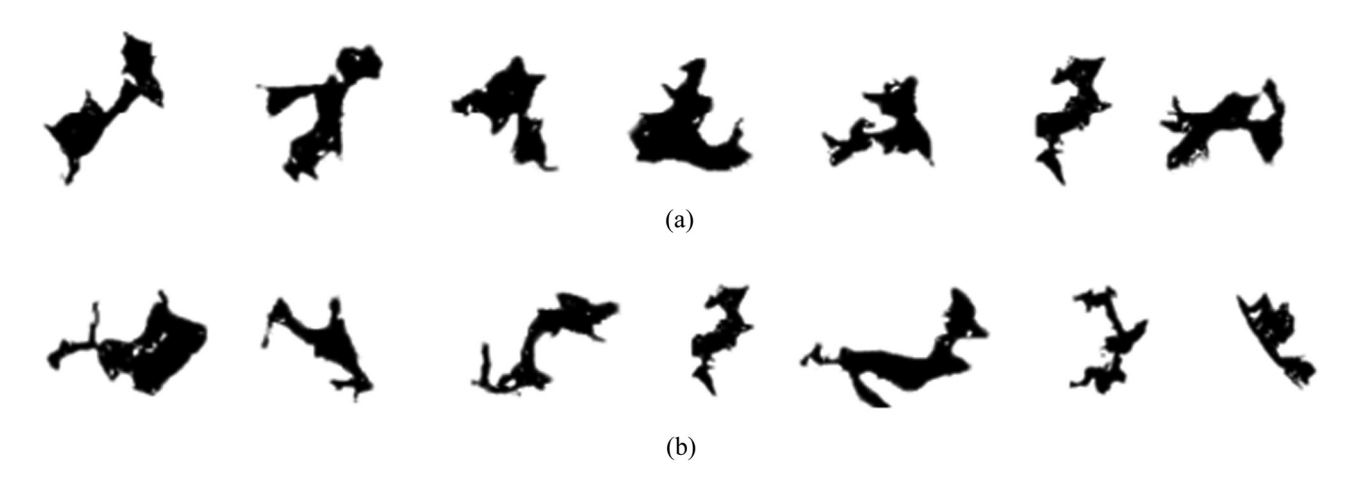


Figure 13: Morphology extraction of cross-section pores: (a) specimen before freeze-thaw cycles and (b) specimen after freeze-thaw cycles.

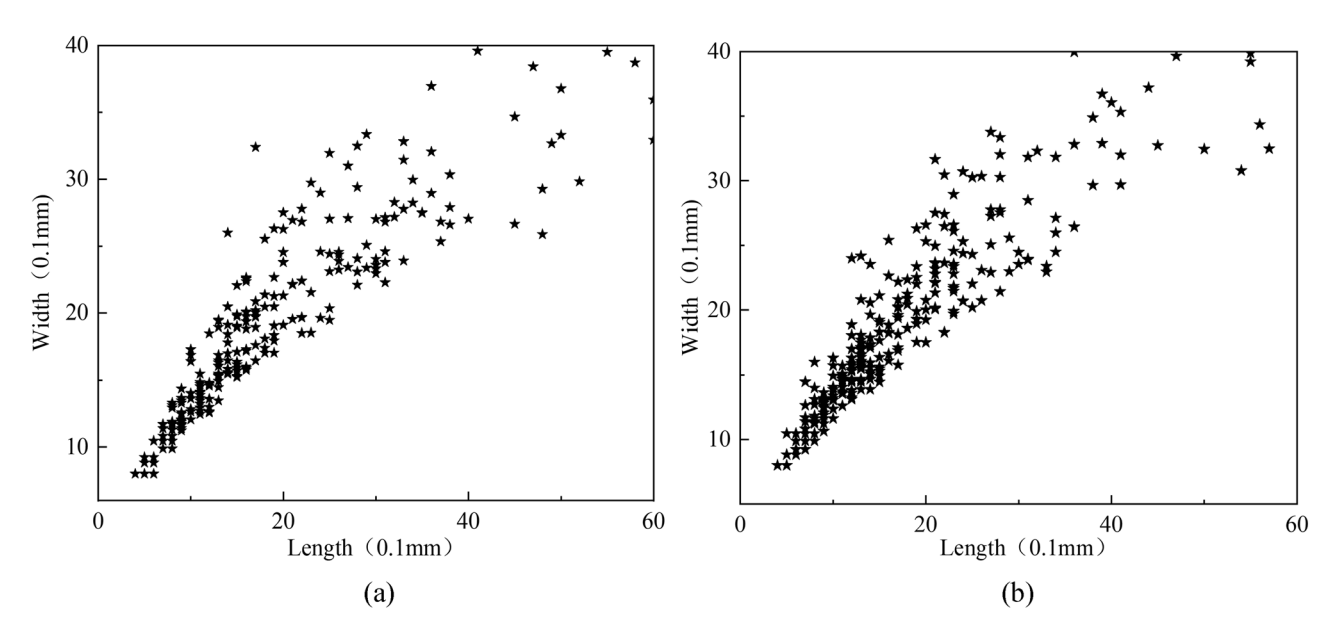


Figure 14: Boundary characteristics of asphalt mixture voids: (a) specimen before freeze-thaw cycles and (b) specimen after freeze-thaw cycles.

freeze-thaw cycle, leading to an increase in void size and, ultimately, deterioration in the performance of the combination.

submerged for 2 h in a 25°C water bath after spending 24 h in a 60°C water bath.

The freeze-thaw cycle process is shown in Figure 15.

#### 5 Macro-experimental analysis

#### 5.1 Freeze-thaw split test

In order to examine the voids of the three graded asphalt mixes under each cycle number, rate, and splitting strength, Marshall specimens were made using two modified asphalts and then exposed to 0, 1, 3, 6, 9, 12, and 15 freeze–thaw cycles. The procedure of the freeze–thaw cycle is as follows: first, perform a 15 min water saturation treatment at a vacuum setting of 98.3−98.7 kPa. By opening the valve and letting the specimen soak in water for 0.5 h, you may return the pressure to normal. The specimen should then be removed, put in a plastic bag with 10 mL of water, and chilled to −18°C for 16 h. The frozen specimen was then

#### 5.2 Analysis of the results of the macroexperiment

#### 5.2.1 Analysis of void ratio change

Marshall specimens of the three graded asphalt mixtures were subjected to multiple freeze—thaw cycles under the two modified asphalts, and their porosity was evaluated after six freeze—thaw cycles. The surface dry technique should be used to measure the porosity of different asphalt mixture specimens with a water absorption rate of less than 2%. As a result, the porosity of AC-13 and SMA-13 with a water absorption rate of less than 2% was evaluated using the surface dry technique, whereas the porosity of PAC-13 with a higher porosity was assessed using the volume method. The formula for calculating the void ratio is shown in following formula:



Figure 15: Freeze-thaw cycle process.

$$VV = (1 - \gamma_f/\gamma_f) \times 100, \tag{4}$$

where VV is the asphalt mixture specimen's porosity (%),  $y_f$  is the dimensionless gross volume relative density of the asphalt mixture, and  $y_t$  is the dimensionless theoretical maximum relative density of the asphalt mixture.

After six freeze—thaw cycles, the porosity of the three graded asphalt mixture specimens was assessed, and the results are shown in Table 7.

The porosity found in Table 7 was used to create a graph showing the relationship between the porosity and the quantity of freeze—thaw cycles, and a polynomial fitting was done on the curve as a result. The curve and fitting outcomes are shown in Figure 16.

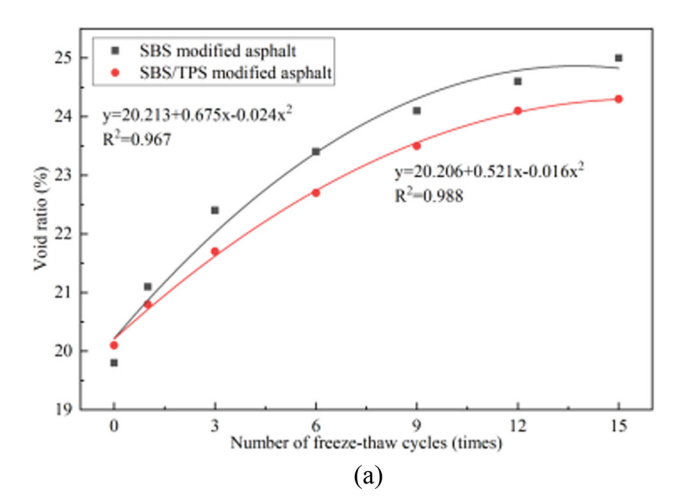
Table 7 and Figure 16 show that as the number of freeze–thaw cycles rises, so do the void percentages of the three graded asphalt mixes underneath the two modified asphalts. The  $R^2$  correlation coefficient of the fitted curve, which shows a substantial curve link between the mixture's porosity and the quantity of freeze–thaw cycles, simultaneously spans from 0.967 to 0.991. This indicates that the asphalt mixture's internal structure was somewhat disturbed by the freeze–thaw cycle, increasing the porosity. The mixture's freeze–thaw cycle breaks down the adhesion between the gravel and asphalt. Lack of adhesion causes the asphalt to slip off the aggregate's surface, and repeated freeze–thaw cycles cause certain small, closed holes to eventually open up into linked pores, raising the asphalt mixture's void ratio.

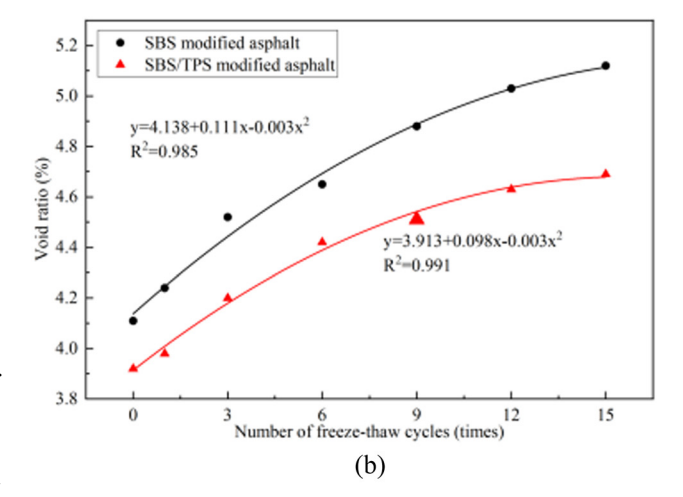
Using the growth ratio of the porosity of the mixture after 15 freeze—thaw cycles as an example, the porosity of PAC-13, SMA-13, and AC-13 increased after 15 freeze—thaw cycles compared to the initial porosity under the SBS-modified asphalt. PAC-13, SMA-13, and AC-13 porosity rose by 20.89, 19.64, and 19.95%, respectively, as compared to SBS-treated asphalt. Asphalt prices dropped by 5.37, 4.93, and 4.11%, respectively. The use of SBS/TPS-modified asphalt improves asphalt cohesion and adhesion between asphalt

**Table 7:** Calculation results of porosity of three graded asphalt mixtures after freeze–thaw cycles

Types of as mixtures	Poros	sity of a	•	t mixtu cycles (		er freez	e–thaw	
		0	1	3	6	9	12	15
SBS- modified asphalt SBS/TPS- modified asphalt	PAC-13 SMA-13 AC-13 PAC-13 SMA-13 AC-13	19.8 4.11 4.53 20.1 3.92 4.45	21.1 4.24 4.58 20.8 3.98 4.51	22.4 4.52 4.82 21.7 4.2 4.64	23.4 4.65 4.97 22.7 4.42 4.82	24.1 4.88 5.28 23.5 4.51 5.06	24.6 5.03 5.51 24.1 4.63 5.25	25.0 5.12 5.62 24.3 4.69 5.32

and aggregate, resulting in more tightly wrapped aggregate and asphalt mortar and a more solid overall structure of the combination. Water erosion is difficult to cause





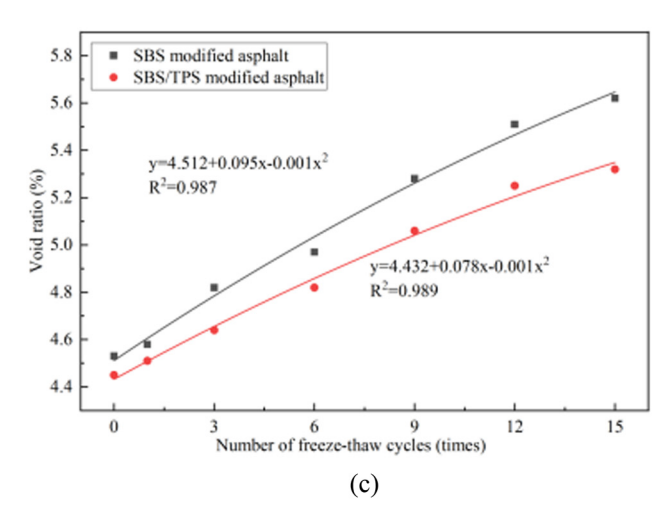


**Figure 16:** Variation of porosity of three graded asphalt mixtures with the number of freeze–thaw cycles: (a) PAC-13 asphalt mixture, (b) SMA-13 asphalt mixture, and (c) AC-13 asphalt mixture.

damage, which increases resistance against water damage. It demonstrates that the porous asphalt mixture modified with SBS/TPS performs better after multiple freeze—thaw cycles, indicating that the use of SBS/TPS-modified asphalt improves the porous asphalt mixture's durability under the influence of freeze—thaw cycles.

#### 5.2.2 Analysis of freeze-thaw split tests result

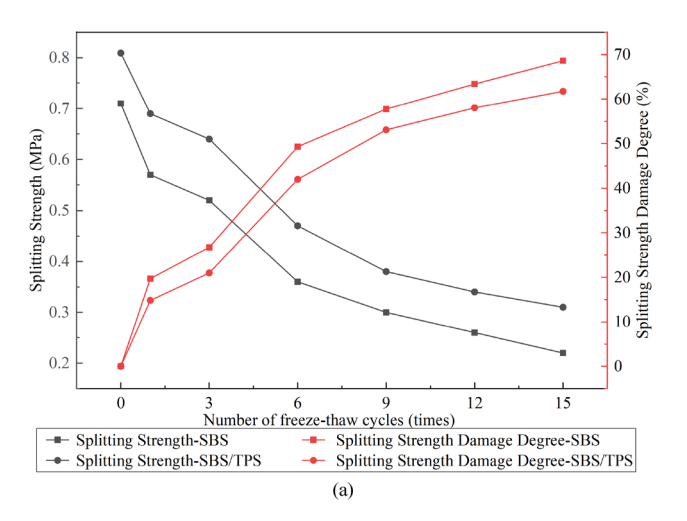
After the specimens had undergone freeze—thaw cycles, they were divided, and the porous asphalt mixture's resistance to freeze—thaw damage was assessed using the split tensile strength. The void growth rate is defined as the void fraction damage degree [30], and its calculation formula is shown in formula (5). This is done in order to quantify the impact of freeze—thaw cycles on the splitting strength of porous asphalt mixtures as well as the durability of asphalt mixtures under freeze—thaw cycles.

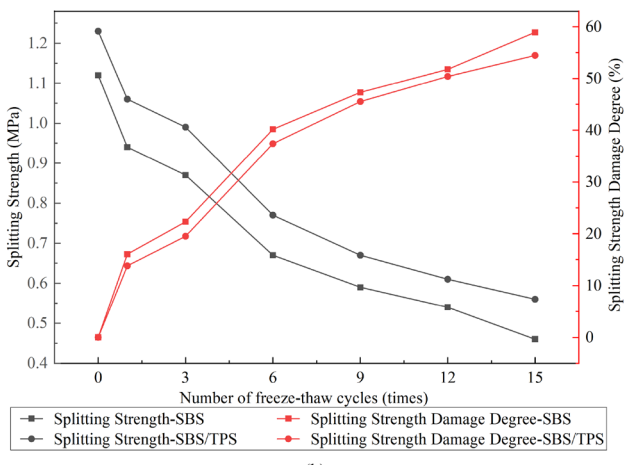
$$D = \frac{V_x - V_0}{V_0} \times 100, \tag{5}$$

**Table 8:** Splitting test results of three graded asphalt mixtures after different freeze–thaw cycles

Туре	Number of cycles	SBS-modif	ied asphalt	SBS/TPS-modified asphalt		
	(times)	Splitting strength (MPa)	Splitting strength damage (%)	Splitting strength (MPa)	Splitting strength damage (%)	
PAC-13	0	0.71	0.00	0.81	0.00	
	1	0.57	19.7	0.69	14.8	
	3	0.52	26.7	0.64	20.9	
	6	0.36	49.2	0.47	41.9	
	9	0.3	57.7	0.38	53.0	
	12	0.26	63.3	0.34	58.0	
	15	0.22	69.0	0.31	61.7	
SMA-13	0	1.12	0.00	1.23	0.00	
	1	0.94	16.0	1.06	13.8	
	3	0.87	22.3	0.99	19.5	
	6	0.67	40.1	0.77	37.3	
	9	0.59	47.3	0.67	45.5	
	12	0.54	51.7	0.61	50.4	
	15	0.46	58.9	0.56	54.4	
AC-13	0	1.08	0.00	1.17	0.00	
	1	0.89	17.5	0.98	16.2	
	3	0.81	25.0	0.91	22.2	
	6	0.62	42.5	0.73	37.6	
	9	0.54	50.0	0.62	47.0	
	12	0.47	56.4	0.54	53.8	
	15	0.41	62.0	0.49	58.1	

where D is the damage degree of porosity (%),  $V_x$  is after x periods, the porosity of the asphalt mixture (%), and  $V_0$  is the asphalt mixture's initial porosity (%).





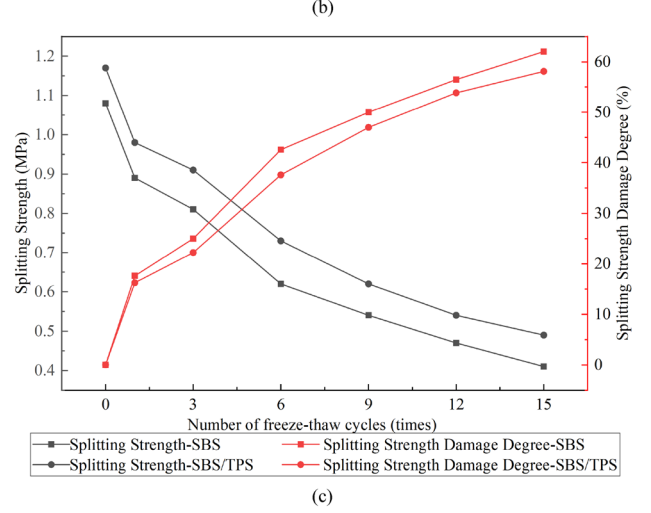


**Figure 17:** Splitting strength and splitting strength loss as a function of the number of freeze–thaw cycles: (a) PAC-13 asphalt mixture, (b) SMA-13 asphalt mixture, and (c) AC-13 asphalt mixture.

Table 9: Comparison of micro, meso, and macro-effect results

Number of freeze-thaw cycles (times)	PAC-13								
	Micro-effect  Interface energy of asphalt–aggregate (kJ·mol <sup>-1</sup> )				Meso-effec	t	Ма	Macro-effect	
				Void area (mm²)	Void ratio change (%)		Split strength (MPa)		
	Original asphalt	SBS- modified asphalt	SBS/TPS- modified asphalt	SBS/TPS- modified asphalt	SBS- modified asphalt	SBS/TPS- modified asphalt	SBS- modified asphalt	SBS/TPS- modified asphalt	
0				1,528	19.8	20.1	0.71	0.81	
1	-2177.2	-3328.1	-3936.5		21.1	20.8	0.57	0.69	
2	-2052.3	-3056.5	-3817.6						
3	-1918.6	-2879.1	-3729.3		22.4	21.7	0.52	0.64	
4	-1853.4	-2614.2	-3614.1						
5	-1632.1	-2314.5	-3534.7	1,745					
6					23.4	22.7	0.36	0.47	
9					24.1	23.5	0.30	0.38	
12					24.6	24.1	0.26	0.34	
15					25.0	24.3	0.22	0.31	

After six freeze—thaw cycles, the splitting strength and splitting strength loss of the three graded asphalt mixture specimens were calculated; the findings are shown in Table 8 and Figure 17.

Table 8 and Figure 17 show that as the number of freeze—thaw cycles increases, the splitting strengths of the three graded asphalt mixes beneath the two modified asphalts all drop, and the decreasing strength trend is consistent with the rising porosity trend. This is consistent with the pattern shown by Fakhri *et al.* using a fracture mechanics approach [31]. Matching, suggesting that the

asphalt mixture's material qualities and structure change to some amount as a result of many freeze—thaw cycles, leading to deterioration in strength, poor durability, and limited service life. The reason is that as the number of freeze—thaw cycles increases, the asphalt mixture is damaged by the long-term coupling of water and temperature, resulting in aging of asphalt, insufficient cohesion and adhesion, and part of the aggregate surface falls off. The pores also gradually expand under water erosion, so that the internal structure of the mixture is damaged to some extent, and finally its splitting strength is gradually reduced.

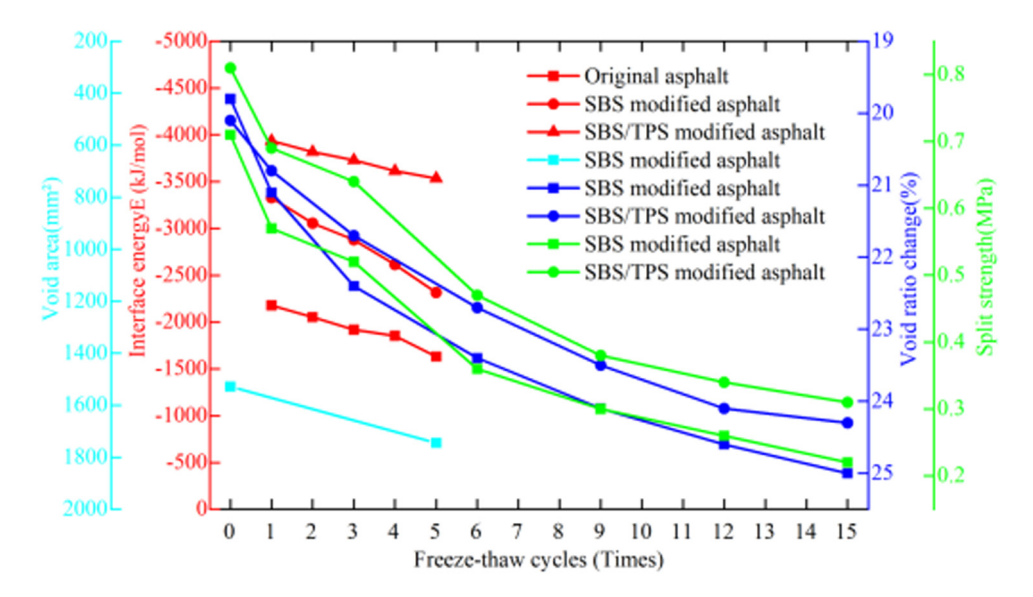


Figure 18: Comparative curve of micro, meso, and macro-effect results (PAC-13).

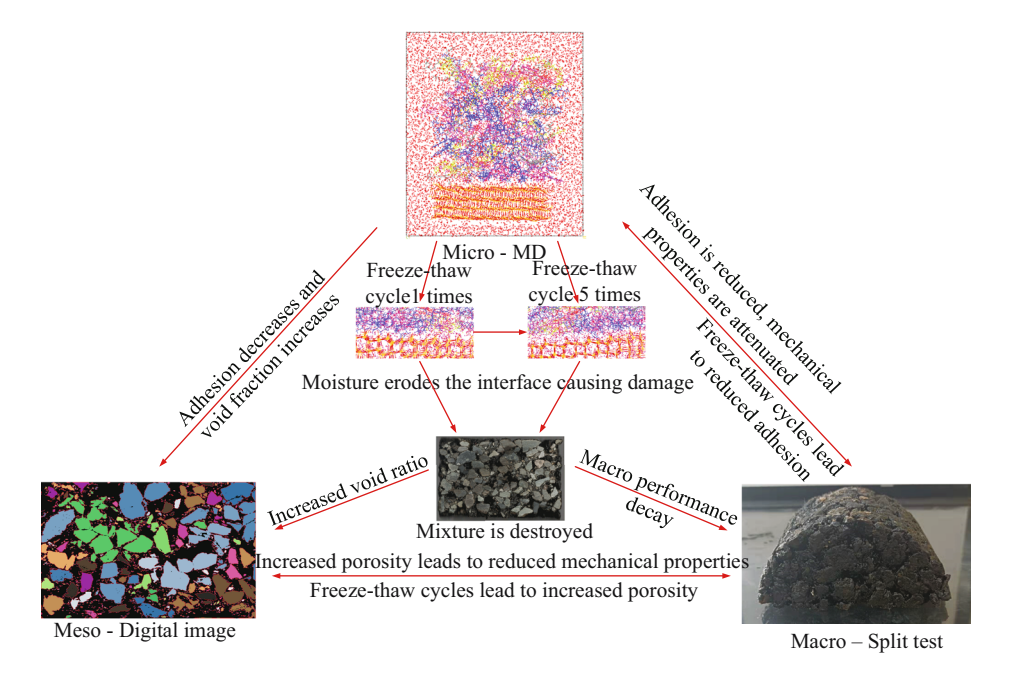


Figure 19: Multi-scale comparison of micro, meso, and macro-effect results (PAC-13).

Using the damage degree of asphalt mixture after 15 freeze—thaw cycles as an example, under SBS-modified asphalt, the damage degree of splitting strength of PAC-13, SMA-13, and AC-13 after 15 freeze—thaw cycles is 69.01, 58.92, and 62.03%, respectively, whereas under high viscosity modified asphalt, the damage degree of splitting strength of PAC-13, SMA-13, and AC-13 is 61.72, 54.47, and 58%. Since the use of high viscosity modified asphalt improves the adhesive force of asphalt and the adhesive force between asphalt and aggregate, the aggregate and asphalt slurry are more tightly wrapped, pores are suppressed, the overall structure is more stable, and water loss resistance is improved.

At the same time, the freeze—thaw splitting strength of the SBS/TPS composite modified asphalt mixture is greater than the freeze—thaw splitting strength of the SBS single modified asphalt mixture. This is because SBS and TPS, the two modifiers in the asphalt will produce swelling effect, and will form a more dense cross-linked mesh structure. In addition, TPS can interact chemically with asphalt to produce a better modification effect, making the modified asphalt have higher viscosity.

Based on the aforementioned analysis, it is evident that as the number of freeze—thaw cycles rises, the internal structure and material properties of the asphalt mixture are continuously harmed. This causes it to be less durable and have a shorter service life. This is consistent with the trend of modulus variation expressed in the microscopic simulations. It was also verified that the decrease in modulus

at the molecular scale causes changes in the macroscopic mechanical properties of the asphalt mixture. This is in agreement with the study of Aliha *et al.* [32] Additionally, after freeze—thaw cycles, the asphalt combination with high viscosity modified asphalt showed stronger strength and less porosity than SBS-modified asphalt.

#### 6 Comparative analysis of multiscale effecting results

# 6.1 Index evolution comparison based on multi-scale effecting results

According to the above effecting results of micro, meso, and macro-structure in part 3, 4, and 5, the three kinds of indexes are collected together and shown in Table 9, and the comparative curve of multi-scale effect results are shown in Figure 18.

Table 9 and Figure 18 show that when the number of freeze-thaw cycles increases, the energy at the asphalt-aggregate interface decreases while the void area and void ratio of the asphalt mixture increase. On the contrary, the freezing-thawing splitting strength diminishes. The progression of the three types of indexes is the same or comparable, and despite the fact that the indexes are different, they all impair the qualities of the combination. As a

result, SBS/TPS-modified asphalt can be employed in the application of porous asphalt mixtures to withstand free-ze-thaw damage.

# 6.2 Comparative discussion of multi-scale effecting results

To sum up, on the basic of above comparative analysis, the mutual effecting mechanism of micro, meso, and macrostructure are shown in Figure 19.

As seen in Figure 19, the MD effect result appropriately explains the meso and macro outcomes. The adhesion of the asphalt-aggregate interface is disrupted at the microscopic level by the freeze-thaw cycles of porous asphalt mixtures. Mesoscopically, when adhesion decreases, the asphalt mixture's void area grows as it slides off the surface of the aggregate. The void ratio increases as the asphalt mixture's freeze-thaw splitting strength decreases on a macroscopic scale. The variation of void area at the fine scale can be explained by the simulation results at the microscopic scale. Microscopic simulation results showed that the freeze-thaw cycling action would gradually reduce the interfacial energy between asphalt-aggregate, and weakened the adhesion between asphalt-aggregate, which makes the fine scale voids in the asphalt mixture. Therefore, there is a correlation between the simulation results at the microscopic scale and the experimental results at the fine scale. To provide a solid foundation for future research on porous asphalt mixes, the effects of freeze-thaw cycles on the performance of porous asphalt mixtures are explored at various scales.

#### 7 Conclusions

- As the frequency of freeze-thaw cycles rises, the energy of the asphalt-aggregate interface drops, enabling more water molecules to flow through and deteriorating asphaltaggregate adhesion. Asphalt's adherence to the aggregate deteriorates. This causes new microscopic gaps to emerge and existing gaps to widen, reducing the performance of the asphalt mixture.
- 2) According to the results of the microscale simulation research, high viscosity modified asphalt had greater adhesion qualities than virgin asphalt and SBS-modified asphalt. It also improved the mechanical properties of the mix after freeze-thaw cycles.
- Freeze-thaw cycles have an impact on the mechanical characteristics of porous asphalt mixtures. The degree

of damage rises as the frequency of freeze—thaw cycles increases. SBS/TPS-modified asphalt greatly enhanced the macromechanical characteristics of mixtures of asphalt under freeze—thaw cycles when compared to the other two asphalts. As a result, the usage of SBS/TPS-modified asphalt, particularly when applied to the porous asphalt combination PAC-13, greatly enhances the material's mechanical qualities during freeze—thaw cycles.

**Acknowledgments:** The authors gratefully appreciate the Supported by the Natural Science Foundation of Heilongjiang Province (LH2022E003) and the supports from the Fundamental Research Funds for the Central Universities (25272022AW56).

Funding information: The authors state no funding involved.

**Author contributions:** All authors have accepted responsibility for the entire content of this manuscript and approved its submission.

**Conflict of interest:** The authors state no conflict of interest.

#### References

- [1] Ling, S., F. Yu, D. Sun, G. Sun, and L. Xu. A comprehensive review of tire-pavement noise: generation mechanism, measurement methods, and quiet asphalt pavement. *Journal of Cleaner Production*, Vol. 287, 2021, id. 125056.
- [2] Jiang, W., Y. Huang, and A. Sha. A review of eco-friendly functional road materials. *Construction and Building Materials*, Vol. 191, 2018, pp. 1082–1092.
- [3] Chu, L. and T. F. Fwa. Functional sustainability of single-and doublelayer porous asphalt pavements. *Construction and Building Materials*, Vol. 197, 2019, pp. 436–443.
- [4] Takahashi, S. Comprehensive study on the porous asphalt effects on expressways in Japan: based on field data analysis in the last decade. *Road Materials and Pavement Design*, Vol. 14, No. 2, 2013, pp. 239–255.
- [5] Zheng, C., J. Xu, T. Zhang, and G. Tan. Study on the microscopic damage of porous asphalt mixture under the combined action of hydrodynamic pressure and ice crystal frost heave. *Construction and Building Materials*, Vol. 303, 2021, id. 124489.
- [6] Wang, Y., H. Zhang, and Q. Zhao. Micro-structural analysis on stress displacement and crack evolution of porous asphalt mixture based on DEM. Materials Research Express, Vol. 8, No. 6, 2021, id. 065102.
- [7] Meiarashi, S., F. Nakashiba, H. Niimi, M. Hasebe, and T. Nakatsuji. Quantitative comparison between noise reduction factors of drainage asphalt pavement. *Applied Acoustics*, Vol. 44, No. 2, 1995, pp. 165–179.
- [8] Dreelin, E. A., L. Fowler, and C. R. Carroll. A test of porous pavement effectiveness on clay soils during natural storm events. *Water Research*, Vol. 40, No. 4, 2006, pp. 799–805.

- [9] Goh, S. W. and Z. You. Mechanical properties of porous asphalt pavement materials with warm mix asphalt and RAP. *Journal of Transportation Engineering*, Vol. 138, No. 1, 2012, pp. 90–97.
- [10] Shirini, B. and R. Imaninasab. Performance evaluation of rubberized and SBS modified porous asphalt mixtures. *Construction and Building Materials*, Vol. 107, 2016, pp. 165–171.
- [11] Chen, J. S., C. T. Lee, and Y. Y. Lin. Influence of engineering properties of porous asphalt concrete on long-term performance. *Journal of Materials in Civil Engineering*, Vol. 29, No. 4, 2017, id. 04016246.
- [12] Islam, M. R., A. Rahman, and R. A. Tarefder. Open graded friction course in resisting low-temperature transverse cracking in asphalt pavement. *Journal of Cold Regions Engineering*, Vol. 32, No. 2, 2018, pp. 04018006.1–04018006.7.
- [13] Xu, G., J. Fan, T. Ma, W. Zhao, X. Ding, and Z. Wang. Research on application feasibility of limestone in sublayer of double-layer permeable asphalt pavement. *Construction and Building Materials*, Vol. 287, 2021, id. 123051.
- [14] Yang, Z., L. Wang, B. Xu, S. Li, D. Cao, B. Yuan, et al. Study of the durability of a fully permeable asphalt pavement structure based on the accelerated pavement test method under saturated conditions. *Journal of Transportation Engineering, Part B: Pavements*, Vol. 148, No. 1, 2022, id. 04021081.
- [15] Aliha, M. R. M., H. Fazaeli, S. Aghajani, and F. M. Nejad. Effect of temperature and air void on mixed mode fracture toughness of modified asphalt mixtures. *Construction and Building Materials*, Vol. 95, 2015, pp. 545–555.
- [16] Mansour, T. N. and B. J. Putman. Influence of aggregate gradation on the performance properties of porous asphalt mixtures. *Journal* of Materials in Civil Engineering, Vol. 25, No. 2, 2013, pp. 281–288.
- [17] Slebi-Acevedo, C. J., P. Lastra-González, I. Indacoechea-Vega, and D. Castro-Fresno. Laboratory assessment of porous asphalt mixtures reinforced with synthetic fibers. *Construction and Building Materials*, Vol. 234, 2020, id. 117224.
- [18] Lebens, M. A. and B. Troyer. Porous asphalt pavement performance in cold regions, 2012.
- [19] Ghoreishian Amiri, S. A., G. Grimstad, M. Kadivar, and S. Nordal. Constitutive model for rate-independent behavior of saturated frozen soils. *Canadian Geotechnical Journal*, Vol. 53, No. 10, 2016, pp. 1646–1657.
- [20] Girifalco, L. A. and R. J. Good. A theory for the estimation of surface and interfacial energies. I. Derivation and application to interfacial tension. *The Journal of Physical Chemistry*, Vol. 61, No. 7, 1957, pp. 904–909.

- [21] Tsai, D. H. The virial theorem and stress calculation in molecular dynamics. *The Journal of Chemical Physics*, Vol. 70, No. 3, 1979, pp. 1375–1382.
- [22] Gao, M., H. Zhang, H. Yang, Y. Li, L. Yu, and S. Zhao. Research on surface morphology characteristics and micro-damage mechanism of asphalt mastic based on charge transfer principle. *Construction and Building Materials*, Vol. 391, 2023, id. 131686.
- [23] Li, D. D. and M. L. Greenfield. Chemical compositions of improved model asphalt systems for molecular simulations. *Fuel*, Vol. 115, No. 1, 2014, pp. 347–356.
- [24] Ding, G., X. Yu, F. Dong, Z. Ji, and J. Wang. Using silane coupling agent coating on acidic aggregate surfaces to enhance the adhesion between asphalt and aggregate: a molecular dynamics simulation. *Materials*, Vol. 13, No. 23, 2020, id. 5580.
- [25] VVarveri, A., J. Zhu, and N. Kringos. Moisture damage in asphaltic mixtures. In: *Advances in Asphalt Materials*, Woodhead Publishing, England, 2015, pp. 303–344.
- [26] Yang, Z., C. H. Yu, K. Guo, and M. J. Buehler. End-to-end deep learning method to predict complete strain and stress tensors for complex hierarchical composite microstructures. *Journal of the Mechanics and Physics of Solids*, Vol. 154, 2021, id. 104506.
- [27] Guan, H., J. Li, Y. Yu, M. Chapman, and C. Wang. Automated road information extraction from mobile laser scanning data. *IEEE Transactions on Intelligent Transportation Systems*, Vol. 16, No. 1, 2014, pp. 194–205.
- [28] Qi, Q., Y. Tian, and L. Han. An improved image segmentation algorithm based on the maximum class variance method. In: MATEC Web of Conferences, EDP Sciences, Vol. 309, 2020, id. 03029.
- [29] Wang, W., L. Wang, H. Xiong, and R. Luo. A review and perspective for research on moisture damage in asphalt pavement induced by dynamic pore water pressure. *Construction and Building Materials*, Vol. 204, 2019, pp. 631–642.
- [30] Tian, Z., X. Zhu, X. Chen, Y. Ning, and W. Zhang. Microstructure and damage evolution of hydraulic concrete exposed to freeze–thaw cycles. *Construction and Building Materials*, Vol. 346, 2022, id. 128466.
- [31] Fakhri, M., S. A. Siyadati, and M. R. M. Aliha. Impact of freeze-thaw cycles on low temperature mixed mode I/II cracking properties of water saturated hot mix asphalt: an experimental study. Construction and Building Materials, Vol. 261, 2020, id. 119939.
- [32] Aliha, M. R. M., H. Ziari, B. Mojaradi, and M. J. Sarbijan. Heterogeneity effects on mixed-mode I/II stress intensity factors and fracture path of laboratory asphalt mixtures in the shape of SCB specimen. Fatigue & Fracture of Engineering Materials & Structures, Vol. 43, No. 3, 2020, pp. 586–604.